Anharmonic vibrational eigenfunctions and infrared spectra from semiclassical molecular dynamics

Marco Micciarelli, Riccardo Conte, Jaime Suarez, and Michele Ceotto

Citation: The Journal of Chemical Physics **149**, 064115 (2018); doi: 10.1063/1.5041911
View online: https://doi.org/10.1063/1.5041911
View Table of Contents: http://aip.scitation.org/toc/jcp/149/6
Published by the American Institute of Physics

Anharmonic vibrational eigenfunctions and infrared spectra from semiclassical molecular dynamics

Marco Micciarelli,[a] Riccardo Conte, Jaime Suarez, and Michele Ceotto[b]
Dipartimento di Chimica, Università degli Studi di Milano, via C. Golgi 19, 20133 Milano, Italy

(Received 28 May 2018; accepted 24 July 2018; published online 13 August 2018)

We describe a new approach based on semiclassical molecular dynamics that allows simulating infrared absorption or emission spectra of molecular systems with inclusion of anharmonic intensities. This is achieved from semiclassical power spectra by computing first the vibrational eigenfunctions as a linear combination of harmonic states, and then the oscillator strengths associated with the vibrational transitions. We test the approach against a 1D Morse potential and apply it to the water molecule with results in excellent agreement with discrete variable representation quantum benchmarks. The method does not require any grid calculations, and it is directly extendable to high dimensional systems. The usual exponential scaling of the basis set size with the dimensionality of the system can be avoided by means of an appropriate truncation scheme. Furthermore, the approach has the advantage to provide IR spectra beyond the harmonic approximation without losing the possibility of an intuitive assignment of absorption peaks in terms of normal modes of vibration. *Published by AIP Publishing.*
https://doi.org/10.1063/1.5041911

I. INTRODUCTION

Experimental vibrational spectroscopy is a powerful tool used for countless applications in chemistry and material science. It is routinely complemented by computer simulations which allow rationalizing the absorption peaks observed experimentally.[1,2] The information extracted from these simulations often consists in the assignment of the experimental peaks in terms of vibrations of specific functional groups, especially when dealing with many degrees of freedom as in the case of materials and large molecular systems. Many calculations though provide only harmonic estimates of vibrational energies and motions. However, the harmonic approximation fails in describing high energy vibrations adequately and, in order to fit computational data to experiments, harmonic frequencies have to be often scaled with *ad hoc* procedures[3,4] reducing the level of reliability of the calculations.

In the last decades, considerable efforts have been made to develop classical[5] and quantum theoretical methods able to go beyond the harmonic approximation. Vibrational configuration interaction,[6–9] multi-configuration time dependent Hartree,[10,11] collocation methods,[12–14] perturbative approaches like the second-order vibrational perturbation theory (VPT2),[15,16] path integral molecular dynamics (MD),[17] and quantum Monte Carlo methods[18–20] are popular examples. They can be employed for simulations of vibrational spectra accounting for anharmonicities in both frequency and intensity.

In this context, semiclassical (SC) Molecular Dynamics (MD) is a powerful tool for investigating molecular vibrational zero point and excited eigenenergies. The SC propagator, obtained upon stationary phase approximation of the parent Feynman's path integral representation, is equivalent to the short-time propagator proposed by Van Vleck.[21,22] The original formulation, which mainly suffered from the need to solve a difficult double boundary problem, was rearranged in a more useful way first by Miller with his initial value representation (IVR),[23–26] and then by the likes of Heller, Herman, Kluk, and Kay that provided a more manageable representation of the propagator in terms of coherent states.[27–29] However, the original SCIVR requires dealing with a multidimensional phase-space integration of a real-time oscillatory integrand limiting the range of applicability of the method.

Recent advances have permitted to reduce the number of trajectories required by semiclassical IVR simulations, as well as the dimensionality of the calculations. Techniques like Filinov and generalized Filinov filtering[30–32] and cellular dynamics[33,34] were shown effective in speeding up the convergence of the semiclassical integrations. The same target was achieved by the time averaged version of SCIVR by Kaledin and Miller[35,36] and by techniques developed in our group like the mixed time-averaging SCIVR[37–39] and the multiple coherent (MC) SCIVR.[40–46] Other methods have been introduced to reduce the dimensionality of the semiclassical investigation.[47] This is also the case of hybrid approaches[48] and "divide-and-conquer" (DC) SCIVR techniques.[49,50]

The SC hallmark lies on the possibility to perform quantum dynamics starting from classical trajectories, a feature that gives SC approaches a clear edge in dealing with high dimensional systems. MD is employed to explore the molecular configurational space including regions away from a specific well, providing a reliable description of the global surface also for systems characterized by multiple minima.[51,52] Furthermore, differently from other methodologies based on MD, the

[a]Electronic mail: marco.micciarelli@unimi.it
[b]Electronic mail: michele.ceotto@unimi.it

classical trajectories are not associated with a target temperature so that thermal effects can be added *a posteriori* without running a new simulation. However, semiclassical (power) spectra are calculated from the time evolution of coherent states, and peak amplitudes obtained from these simulations are not necessarily related to absorption intensities. There are actually some relevant examples in the literature of semiclassical computations in which absorption intensities are estimated and compared to the experiments.[47,53,54] However in approaches using a limited number of trajectories, only the eigenvalues of the spectral decomposition of the vibrational Hamiltonian are usually obtained from semiclassical dynamics, with the exception of a recent study in which Ceotto *et al.* outlined a SC approach able to get eigenfunctions and applied it to the case of the CO_2 molecule.[44] This pre-existing method has a main drawback though; i.e., it relies on a grid in configurational space and so it is not suitable for the general treatment of systems with many degrees of freedom.

In this work, we show how to include the calculation of vibrational eigenfunctions into the semiclassical formalism by expanding them on harmonic states. Relying on harmonic states, this method has the advantage to preserve the description of the properties of a system in terms of harmonic ingredients allowing us to perform, in an easy and intuitive way, the assignment of each eigenstate (and absorption peak) in terms of normal modes of vibration. Starting from the knowledge of semiclassical vibrational eigenfunctions, we will show how the new formalism can be used to compute, at any temperature, the IR absorption intensities as well as any other observable that can be represented as a function of the molecular configurational space. The method does not require any grid setups, and it keeps the possibility of application to high dimensional molecular systems and completes the general SC treatment of molecular vibrations.

In the following of this article, the methodology will be derived, tested on a 1D Morse oscillator, and then applied to determine the eigenfunctions and the IR spectrum of the H_2O molecule. The paper ends with some conclusions and perspectives.

II. THEORY

A. Notation and preliminary definitions

We start by considering the standard representation of a molecular system within the ground state Born Oppenheimer (BO) adiabatic approximation in which the wavefunction of nuclei and electrons is decomposed as

$$\Psi_n(\mathbf{r},\mathbf{R}) = \varphi_0(\mathbf{r};\mathbf{R})e_n(\mathbf{R}). \tag{1}$$

Equation (1) allows describing the nuclear motion via the electronic Potential Energy Surface (PES), derived from the ground state energies of the electronic Hamiltonian at each nuclear structure. Within this notation, $\mathbf{r}$ is the vector collecting position and spin coordinates of all electrons, while $\mathbf{R} = \{R_\alpha\}_{\alpha=1}^{3N}$ represents a given molecular configuration with index $\alpha \in \{1_x, 1_y, 1_z, 2_x, 2_y, \ldots, N_z\}$. The adiabatic nuclear motion is governed by the vibrational Hamiltonian operator

$$\hat{H} = \hat{T} + \hat{V} \tag{2}$$

with the potential $V(\boldsymbol{R})$ given by the PES.

If $\mathbf{R}_{eq}$ labels a given configuration of minimum energy on the surface, the second-order approximation to the spectrum of $\hat{H}$ around $\mathbf{R}_{eq}$ is derived by diagonalizing the mass scaled Hessian matrix of the PES in $\mathbf{R}_{eq}$,

$$\sum_{\alpha,\beta} \xi_\beta^\gamma \, U_{\beta\alpha} \, \xi_\alpha^\lambda = \omega_\gamma^2 \, \delta_{\gamma\lambda}, \tag{3}$$

where $U_{\alpha\beta} = \frac{1}{\sqrt{m_\alpha m_\beta}} \frac{\partial^2 V}{\partial R_\alpha \partial R_\beta}|_{\boldsymbol{R}=\boldsymbol{R}_{eq}}$ and ξ_α^λ is the αth component of the λth eigenvector of U. The vibrational Hamiltonian can be conveniently expressed in terms of mass scaled normal mode coordinates centered on the equilibrium geometry,

$$\mathbf{Q} = \mathbf{q} - \mathbf{q}_{eq}, \tag{4}$$

where $\mathbf{q}$ is the vector of normal mode coordinates defined as

$$q_\alpha = \sum_\beta \xi_\beta^\alpha \, R_\beta \sqrt{m_\beta} \tag{5}$$

and $\mathbf{q}_{eq}$ is the normal mode vector corresponding to the equilibrium position $\mathbf{R}_{eq}$. The spectral decomposition of $\hat{H}$ in terms of vibrational bound states

$$\hat{H}|e_n\rangle = E_n|e_n\rangle, \tag{6}$$

beyond the harmonic approximation, can be derived using the time propagation operator

$$\hat{\mathcal{P}}(t) = e^{-\frac{i}{\hbar}\hat{H}t} = \sum_n e^{-\frac{i}{\hbar}E_n t}|e_n\rangle\langle e_n| \tag{7}$$

to compute the recurring time-dependent overlap (also known as the survival amplitude) of the reference state $|\chi\rangle$,

$$I_\chi(t) \equiv \langle\chi|\hat{\mathcal{P}}(t)|\chi\rangle = \sum_n e^{-\frac{i}{\hbar}E_n t}\,|\langle\chi|e_n\rangle|^2, \tag{8}$$

in which the second equality is obtained introducing the representation of the propagator in the basis of the energy eigenvectors reported in Eq. (7). Equation (8) implies that, independently of the specific choice for the reference state $|\chi\rangle$ to evolve, the eigenenergies of $\hat{H}$ can be found by taking the peak positions of the power spectrum of $I_\chi(t)$,

$$\begin{aligned}\tilde{I}_\chi(E) &= \frac{1}{2\pi T}\int_{-T}^{T} dt\langle\boldsymbol{\chi}|\hat{\mathcal{P}}(t)|\boldsymbol{\chi}\rangle e^{\frac{i}{\hbar}Et} \\ &= \frac{1}{\pi T}\,Re\left[\int_0^T dt\langle\chi|\hat{\mathcal{P}}(t)|\chi\rangle e^{\frac{i}{\hbar}Et}\right],\end{aligned} \tag{9}$$

where the tilde symbol indicates the action of the Fourier transform operator. The second equality is simply obtained considering that $\hat{\mathcal{P}}(t) = \hat{\mathcal{P}}^\dagger(-t)$. It is important to stress that the intensity of each peak of $\tilde{I}_\chi(E_n)$ is proportional to the square modulus of the projection of the reference state $|\chi\rangle$ onto the corresponding eigenstate $|e_n\rangle$, as shown in Eq. (8). These quantities, in which the quantum propagator is approximated at the semiclassical level of theory, will be central for the following derivations.

B. Energy eigenfunctions in a harmonic basis set

We can now conveniently consider the complete and orthonormal N-dimensional basis set $\{|\phi_{\mathbf{K}}\rangle\}$ obtained from the Hartree product of one-dimensional harmonic states

$$|\phi_{\mathbf{K}}\rangle = |\phi_{\mathbf{K}}^{(1)}, \phi_{\mathbf{K}}^{(2)}, \ \dots \ , \phi_{\mathbf{K}}^{(N_v)}\rangle = |\phi_{\mathbf{K}}^{(1)}\rangle \ \dots \ |\phi_{\mathbf{K}}^{(N_v)}\rangle, \quad (10)$$

where N_v is the number of vibrations of the system ($3N-5$ for linear molecules, $3N-6$ otherwise) and

$$\begin{aligned}\phi_{\mathbf{K}}^{(\alpha)}(Q_\alpha) &= \langle Q_\alpha|\phi_{\mathbf{K}}^{(\alpha)}\rangle \\ &= \frac{1}{\sqrt{2^{K_\alpha}K_\alpha!}}\left(\frac{\omega_\alpha}{\pi\hbar}\right)^{\frac{1}{4}} \times e^{-\frac{\omega_\alpha Q_\alpha^2}{2\hbar}} h_{K_\alpha}\left(\sqrt{\frac{\omega_\alpha}{\hbar}}\, Q_\alpha\right),\end{aligned} \quad (11)$$

where h_{K_α} is the K_α^{th}-order Hermite polynomial. The vibrational eigenstates of the nuclear Hamiltonian can be expanded in this basis set, i.e.,

$$|e_n\rangle = \sum_{\mathbf{K}} C_{n,\mathbf{K}}|\phi_{\mathbf{K}}\rangle, \quad (12)$$

where $C_{n,\mathbf{K}} = \langle\phi_{\mathbf{K}}|e_n\rangle$ are the real expansion coefficients.

According to Eq. (8), the square modulus of the generic coefficient $C_{n,\mathbf{K}}$ can be computed considering that it is proportional to the intensities of the Fourier transform of the recurring time-dependent overlap of the corresponding harmonic state $\phi_{\mathbf{K}}$ at the eigenvalue of the vibrational Hamiltonian, i.e.,

$$\tilde{I}_{\phi_{\mathbf{K}}}(E_n) = |\langle\phi_{\mathbf{K}}|e_n\rangle|^2 = \frac{1}{\pi T}\, Re\left[\int_0^T dt\langle\phi_{\mathbf{K}}|\hat{\mathcal{P}}(t)|\phi_{\mathbf{K}}\rangle e^{\frac{i}{\hbar}E_n t}\right] \quad (13)$$

and hence

$$|C_{n,\mathbf{K}}|^2 = \tilde{I}_{\phi_{\mathbf{K}}}(E_n). \quad (14)$$

This means that just the sign of the coefficients $C_{n,\mathbf{K}}$ remains undetermined. However, it can be gained by considering the following time-dependent overlap:

$$\begin{aligned}I_{\mathbf{0K}}(t) &= (\langle\phi_{\mathbf{0}}| + \langle\phi_{\mathbf{K}}|)\hat{\mathcal{P}}(t)(|\phi_{\mathbf{0}}\rangle + |\phi_{\mathbf{K}}\rangle) \\ &= \sum_n |\langle e_n|(|\phi_{\mathbf{0}}\rangle + |\phi_{\mathbf{K}}\rangle)|^2 e^{-iE_n t},\end{aligned} \quad (15)$$

where $|\phi_{\mathbf{0}}\rangle$ indicates the harmonic ground state. In fact, by Fourier transforming Eq. (15) and using Eq. (14), we get

$$\begin{aligned}\tilde{I}_{\mathbf{0K}}(E_n) &= (C_{n,\mathbf{0}})^2 + (C_{n,\mathbf{K}})^2 + 2\, C_{n,\mathbf{K}}C_{n,\mathbf{0}} \\ &= \tilde{I}_{\phi_{\mathbf{0}}}(E_n) + \tilde{I}_{\phi_{\mathbf{K}}}(E_n) + 2\, C_{n,\mathbf{K}}C_{n,\mathbf{0}}.\end{aligned} \quad (16)$$

Solving Eq. (16) for $C_{n,\mathbf{K}}$ and noting that $C_{n,\mathbf{0}} = sign(C_{n,\mathbf{0}})\sqrt{\tilde{I}_{\mathbf{0}}(E_n)}$ leads to the following equation:

$$C_{n,\mathbf{K}} = sign(C_{n,\mathbf{0}})\frac{\tilde{I}_{\mathbf{0K}}(E_n) - \tilde{I}_{\phi_{\mathbf{0}}}(E_n) - \tilde{I}_{\phi_{\mathbf{K}}}(E_n)}{2\sqrt{\tilde{I}_{\phi_{\mathbf{0}}}(E_n)}}, \quad (17)$$

in which $sign(C_{n,\mathbf{0}}) = \pm 1$ just sets the global sign of $|e_n\rangle$ and it is, hence, irrelevant.

C. Semiclassical calculation of time recurring overlaps of harmonic states

In our SC methodology, we compute the recurring time-dependent overlap using the following working formula:[40]

$$\tilde{I}_\chi^{SC}(E) = \frac{1}{(2\pi\hbar)^{N_v}}\frac{1}{2\pi\hbar T}\sum_{j=1}^{N_s}\left|\int_0^T dt\langle\chi|\mathbf{Q}_t^{(j)}, \mathbf{p}_t^{(j)}\rangle e^{i[S_t^{(j)}+Et+\phi_t^{(j)}]/\hbar}\right|^2, \quad (18)$$

where N_s is the number of vibrational states to compute; $\mathbf{Q}_t^{(j)}$ and $\mathbf{p}_t^{(j)}$ are the classical normal mode displacement and momentum vectors at time t obtained propagating the jth classical trajectory with initial conditions $(\mathbf{Q}_0^{(j)}, \mathbf{p}_0^{(j)})$ under the effect of the classical vibrational Hamiltonian; $|\mathbf{Q}_t^{(j)}, \mathbf{p}_t^{(j)}\rangle$ are coherent states of the form

$$\langle\mathbf{x}|\mathbf{Q}_t, \mathbf{p}_t\rangle = \left(\frac{\det(\boldsymbol{\gamma})}{\pi}\right)^{\frac{N_v}{4}} e^{-\frac{1}{2}(\mathbf{x}-\mathbf{Q}_t)^T\boldsymbol{\gamma}(\mathbf{x}-\mathbf{Q}_t)+\frac{i}{\hbar}\mathbf{p}_t^T(\mathbf{x}-\mathbf{Q}_t)}, \quad (19)$$

where $\boldsymbol{\gamma}$ is the $N_v \times N_v$ diagonal matrix, with diagonal elements equal to the harmonic frequencies $\{\omega_\lambda\}_{\lambda=1}^{N_v}$, $S_t^{(j)}$ is the classical action at time t computed along the trajectory in the spirit of Feynman's formulation of path integral quantum mechanics, and, finally, $\phi_t^{(j)}(\mathbf{Q}_0^{(j)}, \mathbf{p}_0^{(j)})$ is the phase of $C_t^{(j)}(\mathbf{Q}_0^{(j)}, \mathbf{p}_0^{(j)})$, the Herman-Kluk prefactor at time t that accounts for second-order quantum fluctuations around each classical path and which is obtained as[28,55]

$$C_t(\mathbf{Q}_0, \mathbf{p}_0) = \sqrt{\frac{1}{2^{N_v}}\left|\frac{\partial\mathbf{Q}_t}{\partial\mathbf{Q}_0} + \frac{\partial\mathbf{p}_t}{\partial\mathbf{p}_0} - i\hbar\boldsymbol{\gamma}\frac{\partial\mathbf{Q}_t}{\partial\mathbf{p}_0} + \frac{i\boldsymbol{\gamma}^{-1}}{\hbar}\frac{\partial\mathbf{p}_t}{\partial\mathbf{Q}_0}\right|}. \quad (20)$$

The starting point of our SC implementation is the Herman-Kluk propagator in its time averaged version by Kaledin and Miller,[35] which can be used to compute the Fourier transformed time-dependent recurring overlaps ($\tilde{I}_\chi$) but which requires to perform a multidimensional integration over initial conditions in phase space. This is usually achieved by means of Monte Carlo techniques, and the method has been applied successfully to describe the vibrational properties of several molecules, yielding very accurate results upon evolution of about 10^3 trajectories per degree of freedom.[36] In our approach, the computational overhead required to construct the quantum propagator is enormously decreased. In fact, as indicated in Eq. (18), we follow the footsteps of the multiple coherent technique[40] and, rather than relying on a full Monte Carlo sampling of the phase space, the propagator is constructed using only N_s tailored trajectories, i.e., one for each target vibrational state. These trajectories are selected and derived carefully on the basis of the starting harmonic approximation to the Hamiltonian. In particular, the initial position is selected to be in the minimum of the potential (equilibrium position), while the initial velocities are chosen in a way to assign to each normal mode a content of kinetic energy equal to $T_\alpha = (n_\alpha + \frac{1}{2})\hbar\omega_\alpha$. Each trajectory requires to be evolved for a very short time (1–2 ps) without any preliminary equilibration to be performed.

Apart from the evolution of the classical trajectories, calculation of $\tilde{I}_\chi^{SC}(E)$ using Eq. (18) requires evaluating also the

phase of the prefactor reported in Eq. (20). The prefactor depends on the stability matrix elements $\frac{\partial(Q_t^{(\alpha)}, p_t^{(\alpha)})}{\partial(Q_0^{(\alpha)}, p_0^{(\alpha)})}$, which are obtained via numerical integration of their symplectic equations of motion along the classical trajectory.[56] For this purpose, however, the computationally expensive calculation of the instantaneous Hessian matrix $\frac{\partial^2 V}{\partial Q_\alpha \partial Q_\beta}\Big|_{\mathbf{Q}_t}$ is needed. Specific algorithms have been developed to ease computational costs in high dimensional applications by reducing the number of Hessian calls.[57,58] The reference state to evolve is usually chosen to be in the form of a coherent state $|\chi\rangle = |\bar{\mathbf{Q}}, \bar{\mathbf{p}}\rangle$ so that the scalar product $\langle\chi|\mathbf{Q}_t, \mathbf{p}_t\rangle$ can be computed analytically at each phase space point visited during the classical MD. However, for our purposes, we want to consider the case in which $|\chi\rangle = |\phi_{\mathbf{K}}\rangle$. The calculation of the following overlap is then needed:

$$\langle\phi_{\mathbf{K}}|\mathbf{Q}_t, \mathbf{p}_t\rangle = \prod_{\alpha=1}^{N_v} \langle\phi_{\mathbf{K}}^{(\alpha)}|Q_t^{(\alpha)}, p_t^{(\alpha)}\rangle, \tag{21}$$

which has the analytical form

$$\langle\phi_{\mathbf{K}}^{(\alpha)}|Q_t^{(\alpha)}, p_t^{(\alpha)}\rangle = e^{-\frac{i}{2\hbar}Q_t^{(\alpha)}p_t^{(\alpha)}} e^{-\frac{\omega_\alpha}{4\hbar}[Q_t^{(\alpha)}]^2 - \frac{1}{4\omega_\alpha\hbar}[p_t^{(\alpha)}]^2} \times \frac{(\sqrt{\frac{\omega_\alpha}{2\hbar}}\, Q_t^{(\alpha)} + i\sqrt{\frac{1}{2\omega_\alpha\hbar}}\, p_t^{(\alpha)})^{K_\alpha}}{\sqrt{K_\alpha!}}. \tag{22}$$

The details of the analytical derivation of Eq. (22) can be found in Appendix A.

D. Calculation of temperature dependent absorption spectra

Once the spectral decomposition of the vibrational operator has been achieved, the IR absorption intensities can be obtained using quantum linear response theory in its sum-over-state version. Within this formalism, the IR spectrum for isotropic and homogeneous molecular systems is written as[59]

$$S(\omega, T) = \sum_{n\neq m} [P_n(T) - P_m(T)] F_{nm} \delta(\omega - \Omega_{nm}), \tag{23}$$

where $\Omega_{nm} = E_m - E_n$ is the difference between vibrational energies, $P_n = e^{-\frac{E_n}{k_B T}}/Z$ is the nth vibrational state population at a given temperature T (with $Z = \sum_n e^{-\frac{E_n}{k_B T}}$ being the partition function), and

$$F_{nm} \propto \Omega_{nm} |\langle\Psi_n|\hat{\mu}|\Psi_m\rangle|^2 = \Omega_{nm} \times \int d\mathbf{R} \int d\mathbf{r} |\varphi_0(\mathbf{r}; \mathbf{R})|^2 e_n(\mathbf{R}) e_m(\mathbf{R}) \mu(\mathbf{r}, \mathbf{R}) \tag{24}$$

are the oscillator strengths, which depend on the full Hamiltonian eigenstates. In the second equality of Eq. (24), we used the BO approximation for the total wavefunction as illustrated in Eq. (1) with the dipole function μ that can be decomposed as

$$\mu(\mathbf{r}, \mathbf{R}) = \sum_\alpha Z_\alpha R_\alpha + e \sum_i r_i = \mu_N(\mathbf{R}) + \mu_e(\mathbf{r}), \tag{25}$$

where $Z_\alpha \in \{Z_1, Z_1, Z_1, \ldots, Z_N, Z_N, Z_N\}$ is the charge associated with the αth degree of freedom of the system and e is the charge of the electron. The separable form of the dipole operator in Eq. (25) allows computing the oscillator strengths as matrix elements over vibrational states, i.e.,

$$F_{nm} \propto \Omega_{nm} | < e_n | \hat{\mu}_{0N} | e_m > |^2, \tag{26}$$

where

$$\hat{\mu}_{0N}(\mathbf{R}) = \hat{\mu}_N(\mathbf{R}) + \hat{\mu}_{e0}(\mathbf{R}) \tag{27}$$

and

$$\mu_{e0}(\mathbf{R}) = \int d\mathbf{r}\, |\varphi_0(\mathbf{r}; \mathbf{R})|^2 \mu_e(\mathbf{r}), \tag{28}$$

is the electronic dipole associated with a given nuclear configuration. Using Eq. (26), the absorption intensities can be obtained by computing the following integral over the nuclear configurational space:

$$M_{nm} = \int d\mathbf{Q}\, e_n(\mathbf{Q}) e_m(\mathbf{Q}) \mu_{0N}(\mathbf{Q}), \tag{29}$$

the only unknown term being the electronic dipole of Eq. (28) that demands for an electronic structure calculation at every nuclear configuration.

Calculation of these integrals can be approached through a Monte Carlo sampling. This can be done by taking advantage from the fact that, in the expansion of vibrational eigenstates in the harmonic basis of Eq. (11), the Gaussian term (present in each harmonic function) can be factorized out leading to

$$e_n(\mathbf{Q}) = G(\mathbf{Q}, \omega) \sum_{\mathbf{K}} C_{n,\mathbf{K}}\, \bar{\phi}_{\mathbf{K}}(\mathbf{Q}), \tag{30}$$

where $G(\mathbf{Q}, \omega) = e^{-\frac{1}{2\hbar}\mathbf{Q}^T \boldsymbol{\omega}\, \mathbf{Q}}$ is the N_v-dimensional Gaussian term and $\bar{\phi}_{\mathbf{K}}(\mathbf{Q}) = \prod_{\alpha=1}^{N_v} \frac{1}{\sqrt{2^{K_\alpha} K_\alpha!}} \left(\frac{\omega_\alpha}{\pi\hbar}\right)^{\frac{1}{4}} h_{K_\alpha}\left(\sqrt{\frac{\omega_\alpha}{\hbar}}\, Q_\alpha\right)$ is the coordinate representation of the harmonic state $|\phi_{\mathbf{K}}\rangle$ without the Gaussian terms. The integral in Eq. (29) can be conveniently recast in the following way:

$$M_{nm} = \int [d\mathbf{Q}\, G(\mathbf{Q}, 2\omega)] \bar{e}_{nm}(\mathbf{Q})\, \mu_{0N}(\mathbf{Q}), \tag{31}$$

where

$$\bar{e}_{nm}(\mathbf{Q}) = \left(\sum_{\mathbf{K}} C_{n,\mathbf{K}} \bar{\phi}_{\mathbf{K}}(\mathbf{Q})\right)\left(\sum_{\mathbf{K}'} C_{m,\mathbf{K}'} \bar{\phi}_{\mathbf{K}'}(\mathbf{Q})\right). \tag{32}$$

Written as in Eq. (31), this integral is particularly well suited for Monte Carlo sampling. In fact, Gaussian distributions can be easily generated by means of the Box-Muller algorithm[60] so that the integrals can be evaluated as

$$M_{nm} = \mathcal{K} \lim_{N_{MC}\to\infty} \frac{1}{N_{MC}} \sum_{k=1}^{N_{MC}} \bar{e}_{nm}(\mathbf{Q}_k)\, \mu_{0N}(\mathbf{Q}_k), \tag{33}$$

where $\{\mathbf{Q}_k\}$ is a set of molecular configurations generated along the multivariate Gaussian distribution $\mathcal{N}(\mathbf{Q}, \sqrt{\frac{1}{2}\omega^{-1}})$ and

$$\mathcal{K} = \frac{G(\mathbf{Q}, 2\omega)}{\mathcal{N}(\mathbf{Q}, \sqrt{\frac{1}{2}\omega^{-1}})} = \sqrt{\frac{(2\pi)^{N_v}}{2|\omega|}}. \tag{34}$$

III. RESULTS AND DISCUSSIONS

A. 1D Morse oscillator

A good test of performances, accuracy, and features of our methodology is represented by the 1D Morse oscillator. In fact, this model system, even if very simple, contains the level of anharmonicity that is typically encountered in the description of molecular bond stretchings. Within the Morse potential functional form $V(Q) = D_e\left[1 - e^{-\sqrt{\omega^2/2D_e}Q}\right]^2$, we set $\omega = 0.020$ *a.u.* and $D_e = 0.174$ *a.u.* with the aim to mimic the bond vibration of the H_2 molecule. Five classical trajectories $\{Q_t^{(n)}, p_t^{(n)}\}_{n=0,\ldots,4}$ were propagated with initial conditions $Q_0^{(n)} = 0$ and $p_0^{(n)} = \sqrt{(2n+1)\omega}$ in order to describe the first five vibrational states (ground state plus first four excited states) with our SC propagator. These trajectories have been obtained via numerical integration of the classical equations of motion directly in normal modes and using a fourth-order symplectic numerical integrator.[56] Gradients and Hessians were computed numerically through central finite difference formulae.[61]

The generic nth vibrational eigenenergy has been obtained following the prescription of Eq. (18), calculating the Fourier transform of the time recurrent overlap of the nth harmonic state, and extracting the frequency that corresponds to the nth peak position (results are shown in Table S1 of the supplementary material). The semiclassical values thus obtained are very close to the reference analytical values $E_n = (n + \frac{1}{2})\hbar\omega - [\hbar\omega(n + \frac{1}{2})]^2/4D_e$, with errors of the order of the wavenumber up to the second excited state and of a few dozens of cm^{-1} for higher energy states. The Morse eigenfunctions were expanded in terms of the first 10 harmonic eigenstates using Eq. (17) and compared with their analytical expression: $e_n(Q) = N_n\, z(Q)^{\lambda-n-\frac{1}{2}}\, e^{-\frac{1}{2}z}\, L_n^{\alpha}(z(Q))$, where $\lambda = \frac{2D_e}{\hbar\omega}$, $z(Q) = 2\lambda\, e^{-y(Q)}$, $y(Q) = \sqrt{\frac{\omega^2}{2D_e}}\, Q$, $\alpha = 2\lambda - 2n - 1$, $L_n^{\alpha}(z)$ is the generalized Laguerre polynomial, and N_n are their normalization constants (derived by means of numerical integration).

On the left column of Fig. 1, we report the first three SC vibrational eigenfunctions together with the corresponding exact and harmonic wavefunctions. As for the ground state eigenfunction, it is evident that the anharmonic corrections are minor and the harmonic approximation already provides a realistic guess. However, it fails in locating the maximum of the wavefunction, which shifts from the harmonic estimate ($Q = 0$) to $Q \sim 3$ a.u. in mass-scaled coordinates (or about 0.05 Å in Cartesian coordinates) in the direction of bond cleavage when the anharmonicity of the potential is properly accounted for. Interestingly, this effect is already correctly described when truncating the harmonic basis set at the level of the first excited state. The corresponding coefficient (C_{01} in our notation) has an amplitude of ∼0.1, and the sign of this coefficient gives the direction of the shift. If a bigger harmonic basis set is employed, only two other coefficients provide a non-negligible but minor contribution of the order of the percent.

The effects of anharmonicity become more and more relevant as the vibrational energy increases. SC dynamics

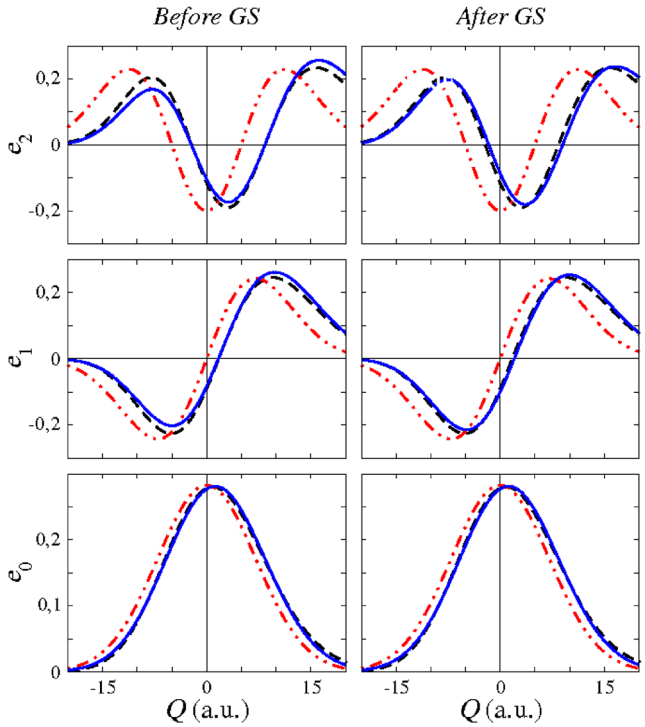

FIG. 1. Semiclassical eigenfunctions (blue continuous lines) for the ground, first, and second excited state of a 1D-Morse potential upon expansion on a basis set made of the first 10 harmonic eigenstates. Results are compared with the corresponding harmonic (red double-dotted-dashed lines) and exact (black dashed lines) ones. On the right side column, the wavefunctions are refined using the Gram Schmidt algorithm, while on the left hand side, they are reported before the "*a posteriori*" orthogonalization. The mass-scaled coordinates are in a.u.

performs better than the harmonic approximation in all cases but, starting from $e_2(Q)$, discrepancies between SC and exact wavefunctions become evident (see Fig. S1 of the supplementary material). The quality of the eigenfunctions can be improved by imposing the orthonormalization condition to the SC wavefunctions after their basic, preliminary estimate obtained via Fourier transform of the recurring overlap. This can be done efficiently using the Gram Schmidt (GS) algorithm. Application of the GS scheme is straightforward and constitutes a simple post-processing refinement of the results. Furthermore, by construction, the GS algorithm does not manipulate the ground state wavefunction where the anharmonic corrections are minor and efficiently accounted for. Wavefunctions are then improved iteratively starting from the ground state in a way that orthogonality is enforced only against wavefunctions already optimized. As demonstrated by the right column of Fig. 1, the procedure permits to escalate the quality of the SC wavefunctions which is now not only excellent up to $e_2(Q)$ but also very good for $e_3(Q)$ and $e_4(Q)$ (as reported in Fig. S1 of the supplementary material).

A quantitative estimate of the accuracy reached with our method has been obtained with the calculation of selected non-vanishing nuclear transition dipoles $d_{nm} = \langle e_n|Q|e_m\rangle$. We computed them numerically on a uniform grid of 10^4 points using the SC eigenfunctions and compared the results with exact analytical values given by the following equation:

TABLE I. 1D-Morse oscillator dipoles (in a.u.) for selected (non-vanishing) vibrational transitions. The transitions are reported in the first column. Numerical estimates obtained using our method are reported before and after the application of the GS procedure and are compared with their analytical values derived from Eq. (35).

Transition dipoles	Before GS SC	After GS SC	Exact
d_{01}	0.16	0.16	0.17
d_{12}	0.25	0.24	0.25
d_{13}	0.01	0.05	0.04
d_{23}	0.34	0.30	0.31
d_{24}	0.01	0.07	0.06
d_{34}	0.42	0.35	0.36

$$d_{mn}^{(ex)} = \frac{2(-1)^{m-n+1}}{(m-n)(2K-n-m)} \times \sqrt{\frac{(K-n)(K-m)\,\Gamma(2K-m+1)m!}{\Gamma(2K-n+1)n!}}, \quad (35)$$

where $K = \lambda - \frac{1}{2}$. Results are reported in Table I. Transition dipoles $0 \to 1$ and $1 \to 2$ are accurate within a tolerance of 0.01 a.u. even before the GS refinement, confirming that the quality of the ground state and first two excited SC wavefunctions is very high. The dipoles associated with excitations involving higher energy states ($1 \to 3$, $2 \to 3$, $2 \to 4$, $3 \to 4$) are instead less accurate, and SC results are correct only within a tolerance of 0.05 a.u. However, after GS orthonormalization, the quality of these exotic transition dipoles improves and their accuracy becomes comparable to that of dipoles involving lower energy states.

B. H_2O molecule

We now move to apply our method to the description of the vibrations of the non-rotating water molecule in vacuum. We employed in our calculation a pre-existing analytical PES based on a quartic force field involving the displacement coordinates of the internal angle and the two bonds.[62] First, the Hessian matrix has been diagonalized to find the three harmonic frequencies of vibration, which are well known to be related to the symmetric stretch (ω_s = 3831 cm^{-1}), the bending (ω_b = 1650 cm^{-1}), and the asymmetric stretch (ω_a = 3941 cm^{-1}) motions. Consistent to the case of the Morse oscillator, five classical trajectories, corresponding to the harmonic states (in increasing order of energy) (0,0,0), (0,1,0), (0,2,0), (1,0,0), (0,0,1), have been run to determine the 5 lowest-lying vibrational states of water semiclassically. These trajectories have been evolved by means of the same symplectic numerical integrator adopted for the Morse oscillator with gradients and Hessians calculated through the usual central finite-difference scheme.

Reference quantum molecular dynamics calculations were carried out by means of the Grid Time-Dependent Schrödinger Equation (GTDSE) computational package.[63] The GTDSE code includes an implementation of the Lanczos algorithm[64–66] that we exploited to extract the eigenfunctions and eigenvalues of the Hamiltonian. The space of coordinates was discretized, and finite difference methods[61] were employed to calculate the derivatives required by the Laplacian operator. The accuracy of the calculations depends on the density of the grid points in the discretization and on the number of points (stencil) used to calculate the derivatives. The finite difference scheme is formally equivalent to discrete variable representation (Sinc-DVR) methods when including all the grid points in the stencil,[67] although this is usually unnecessary since the convergence is rapidly reached. This feature makes the GTDSE particularly efficient in the case of a (generalized) Cartesian coordinate system, where the second derivatives in the Laplacian return a sparse Hamiltonian matrix. In order to better compare these DVR results with SC ones for H_2O, we used the Lanczos algorithm and represented both the PES and the wavefunctions directly in the same normal mode coordinates as the semi-classical calculations, with grid limits $L_i = \pm 75.0$ a.u. (i = 1, 2, 3) for the mass-scaled $\boldsymbol{Q}_i$ coordinates, using 150 grid points and 15 points in the stencil along each direction. An additional benchmark calculation, this time in Jacobi coordinates, was used to extract the DVR vibrational reference values for the non-rotating molecule ($\mathbf{J} = 0$). These eigenenergies, together with more details about this system of coordinates, are reported in the supplementary material (see Table S12).

In Fig. 2, we report the plots of $\tilde{I}_{\phi_\mathbf{K}}(E)$ for the first five harmonic states of water. The semiclassical vibrational energies derived from the positions of the peaks lay within ~30 cm^{-1} of the reference DVR estimates on the same PES and normal coordinate system. A similar level of accuracy was obtained by Kaledin and Miller propagating coherent states.[35] This result confirms the quality of the MC-SCIVR approximation independently of the particular reference state (harmonic or coherent) propagated.

For a general N_v-dimensional system, the size of the (truncated) harmonic basis set, obtained considering all the

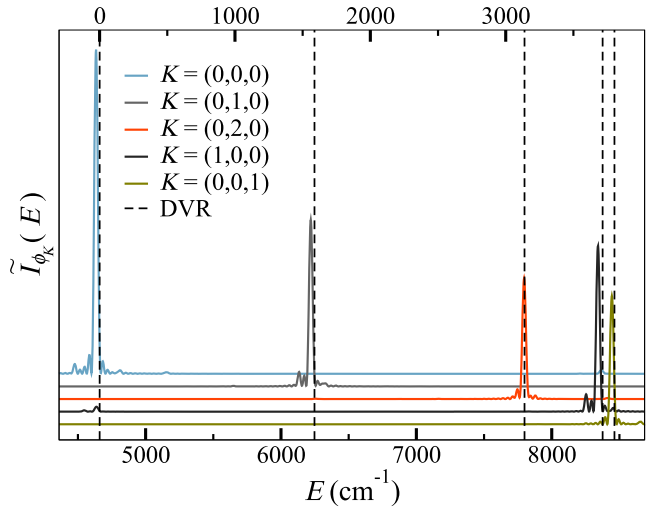

FIG. 2. Fourier transforms of the recurring time dependent overlaps ($\tilde{I}_{\phi_\mathbf{K}}(E)$) obtained evolving the five least energetic harmonic states with the SC propagator, constructed using a single trajectory with the corresponding harmonic energy. The power spectra are shifted in the ordinate axis in order to facilitate visualization and reported in different colors (indicated in the legend). Reference DVR energy values for the normal coordinates system are presented with dashed vertical black lines. The upper horizontal axis reports the shift in frequency (cm^{-1}) from the zero point energy (ZPE) peak.

possible N_v-dimensional direct products of 1-dimensional harmonic eigenstates up to the quantum number k_{max}, is $(k_{max} + 1)^{N_v}$, and hence it grows exponentially with the number of vibrational degrees of freedom. This issue makes the description of vibrational wavefunctions of medium-size or larger molecular systems (i.e., when $N_v \sim 10$ or bigger) virtually undoable because the dimension of the basis set would be too large to be stored in a computer. This is not the case for the water molecule ($N_v = 3$) and hence, expanding the eigenfunctions in terms of the first 11 harmonic states ($k_{max} = 10$), the total number of states in the basis set adds up to just $11^3 = 1331$. Even if such a calculation for water is feasible, in view of future applications of this method to molecules of higher dimensionality, we reduced the amount of data to be stored by setting all coefficients with amplitude smaller than 0.01 to zero. The surviving coefficients were refined by enforcing orthonormality by means of the GS algorithm. In this way, the ground state eigenfunction was decomposed on just five harmonic states, while excited states are required to increase the basis set size up to about 10 elements.

The eigenfunctions are plotted in three different cuts of the configurational space in Fig. 3 where they are also compared with their reference DVR estimate. The accuracy obtained is very high for all cases and the effect of the truncation of the basis set is barely visible on the nodal planes where the SC wavefunctions are slightly overstructured. In perspective, this procedure can help overcome the curse of dimensionality given by the exponential growth of the size of the harmonic basis as a function of the system dimensionality. In fact, in order to moderate the number of harmonic states to generate, a polynomial growth can be enforced, for instance, by building an initial basis set which includes only states with a maximum of simultaneously excited degrees of freedom smaller than N_v. An alternative approach would consist in selecting the harmonic states in the basis set under a constraint on the total energy, which has to be close to the desired target energy. Then, the same procedure adopted for H_2O can be applied on this basis set of reduced size.

Anharmonicity effects for the bending and asymmetric stretching modes are small because all odd order terms in the PES force field vanish for symmetry. However, two main effects that characterize the H_2O molecule are efficiently accounted for by this method. The first one involves the symmetric stretch mode along which the potential is approximately the sum of two Morse-like 1D potentials for the OH bond stretching. Consistently with the case of the 1D Morse oscillator, the anharmonicity generates a coefficient $C_{0,(100)}$ of the order of 10% in the expansion of the ground state wavefunction (see Table S7 of the supplementary material), shifting the maximum with respect to the harmonic eigenfunction in the direction of the dissociation. This effect is clearly visible in Fig. 4.

The second relevant anharmonicity effect regards the presence of a Fermi resonance between the harmonic states corresponding to a double excitation of the bending (i.e., state ϕ_{020}) and the first excited state for the symmetric stretch ϕ_{100}. In terms of expansion coefficients, this effect is pointed out by the presence of two non-negligible terms $C_{2,(100)} \sim C_{3,(020)} \sim 0.15$ for the second and third anharmonic states (see Tables S9 and S10 of the supplementary material). The Fermi resonance is well represented in Fig. 4. Its effect on the shape of the anharmonic eigenfunction e_2 is clearly visible in the bidimensional contour plot reported in panel (a). In fact, there is a distortion of the harmonic symmetry in the direction of negative Q_2 values where, as shown in (f), the harmonic ϕ_{100} wavefunction is positive. The anharmonic distortions of state

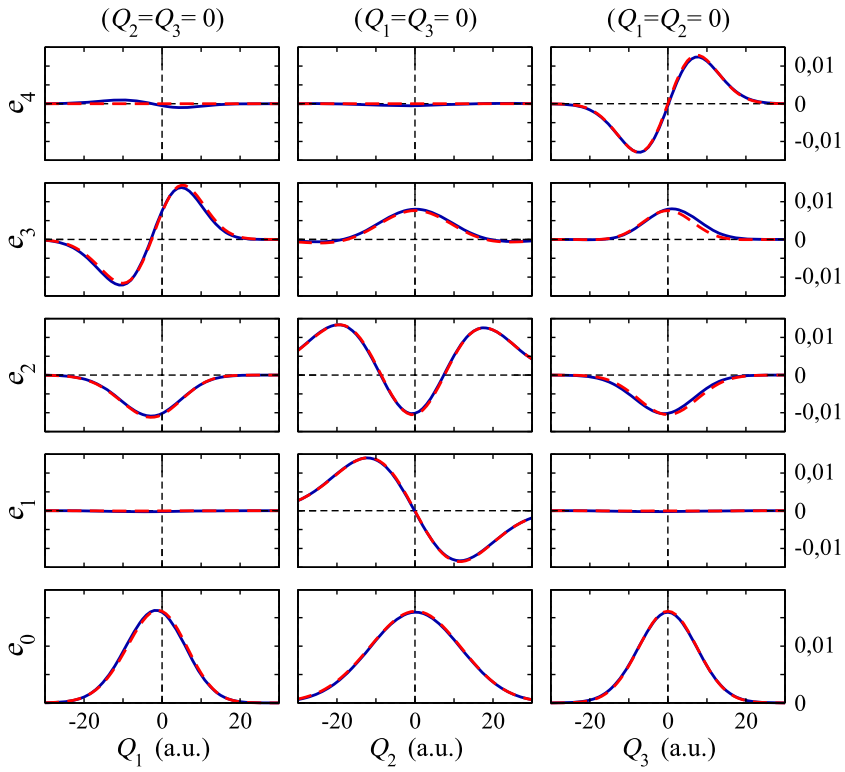

FIG. 3. Selected cuts of the water eigenfunctions obtained by means of DVR (in red) and with SC dynamics (in blue). The cuts are performed on the three directions of the configurational space derived by fixing two of the three normal coordinates at their equilibrium values. Wavefunctions are presented in ascending order of energy (from bottom to top) for states (0,0,0), (0,1,0), (0,2,0), (1,0,0), and (0,0,1).

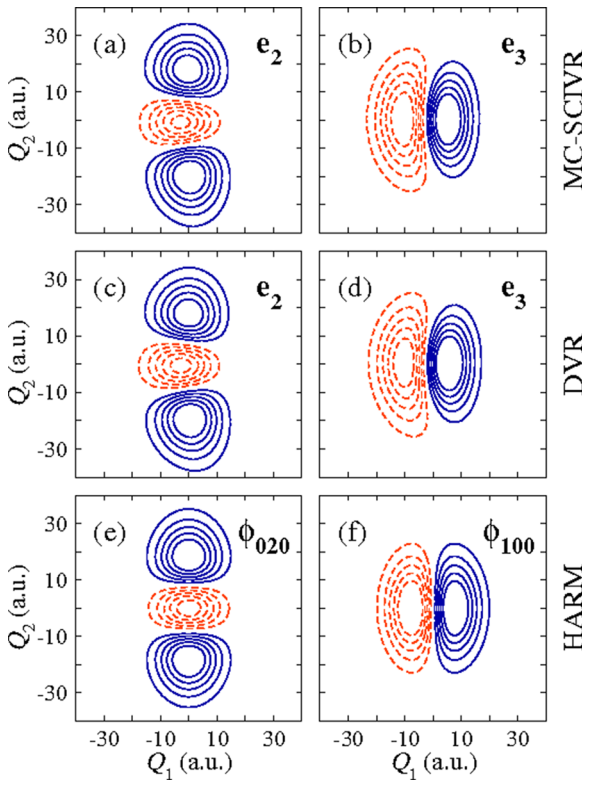

FIG. 4. Bidimensional contour plots of H_2O vibrational eigenfunctions obtained setting $Q_3 = 0$. The pristine harmonic states ϕ_{020} and ϕ_{100} are reported on the bottom row. They are the harmonic approximation to the quantum states e_2 and e_3 plotted in the first (MC-SCIVR estimate) and second row (DVR reference).

e_3 due to the Morse-like shape of the bond stretch potential are also visible in panel (b), which has a broader decay in the direction of dissociation (negative Q_2), opposite to the steeper decay in the direction of positive Q_2, where the potential grows more rapidly because of the repulsive interactions. Excellent overall agreement of the SC wavefunctions [panels (a) and (b)] with their DVR counterparts [panels (c) and (d)] is confirmed also by this plot.

This qualitative agreement between SC and DVR eigenfunctions has been confirmed quantitatively by computing the oscillator strengths by means of Eq. (26). The total dipole moment and the wavefunctions were integrated along the grid of normal mode coordinates. The nuclear component of the dipole moment is readily available, while the electronic part was extracted from the fitted dipole surface of Lodi *et al.*[68] The surface was built in a way that the two components of the electronic dipole moment are returned parallel and perpendicular to the bond-angle bisector vector, while the oxygen atom is set at the origin of the reference frame. For a correct evaluation of the total dipole moment, the electronic and nuclear dipole contributions had to be calculated in the same frame and using the same pole. Results, reported in Table II, confirm the high level of accuracy obtained with the SC wavefunctions with a tolerance of the same order of the one obtained for the 1D Morse potential. Interestingly, due to the presence of the Fermi resonance, the DVR oscillator strength of the bending overtone transition (F_{02}) is of the order of 1% of the fundamental symmetric stretch transition (F_{03}) and not exactly zero (as

TABLE II. The numerical values obtained for the oscillator strengths of water evaluated on the DVR grid are reported in the second and third column using SC and DVR eigenfunctions, respectively. Monte Carlo estimates, obtained by employing the SC eigenfunctions to generate molecular configurations in the MC scheme depicted in Eq. (31), follow in columns 4 and 5. The MC values are reported after the evaluation of the molecular dipole on 25 000 and 50 000 structures. For these cases, the statistical error (estimated as the square root of the variance) is reported in the parentheses.

Oscillator strength	*SC* Grid	*DVR* Grid	*MC* 25 000 steps	*MC* 50 000 steps
F_{01}	19.3	19.6	17.9(±2.6)	18.5(±1.9)
F_{02}	0.01	0.08	0.1(±0.3)	0.1(±0.2)
F_{03}	7.0	7.1	6.4(±2.8)	5.84(±1.9)
F_{04}	8.81	8.82	9.6(±1.1)	8.98(±0.5)
F_{12}	39.9	39.3	37.0(±7.9)	37.0(±5.6)

it is in the harmonic approximation) since there is a minimal contribution coming from the harmonic dipole $\langle\phi_{000}|\hat{\mu}|\phi_{100}\rangle$. This effect, however, is too small to be observed within our SC method because the amplitude of F_{02} is smaller than the tolerance in the SC estimates.

The same oscillator strengths were also computed through the MC scheme of Eq. (33). Results obtained upon evaluation of the dipole over 25 000 and 50 000 structures are reported in the last two columns of Table II. The errors in the MC simulations were calculated by evaluating the standard deviation of the transition dipole moments. The resulting numerical values are all consistent with the reference grid results within the estimated error. Acceptable values have been obtained after 25 000 MC configurations and are improved when considering 50 000 MC configurations. It is known that the number of points needed in a Monte Carlo simulation grows polynomially with system dimensionality. This implies that calculations of

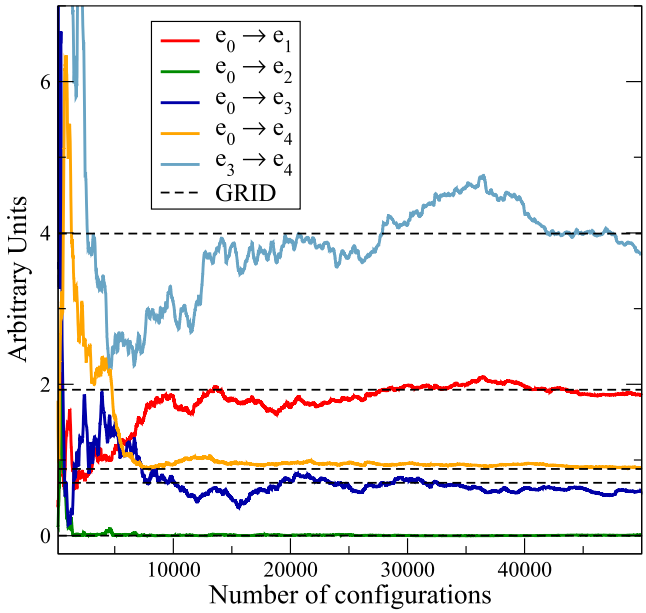

FIG. 5. Running average of the Monte Carlo estimate for the oscillator strengths of selected transitions for the isolated water molecule using Eq. (33). Reference values obtained performing the integral on a numerical grid of 10^6 points are reported as dashed black lines.

this kind can be performed with an affordable computational overhead also for larger systems, where numerical integration on a grid becomes overwhelming. It is worth stressing that the set of Monte Carlo points generated, at which the molecular dipole has to be evaluated, is in common for all transitions. However, convergence is not uniform: as shown in Fig. 5, it is slower for softer vibrations (in this case, the bending) than for harder ones (bond stretching). Moreover, it can be observed that, among stretching mode transitions, the oscillator strength of the asymmetric stretch fundamental excitation ($0 \rightarrow 4$) converges faster than the symmetric one ($0 \rightarrow 3$). This is again due to the presence of the Fermi resonance which affects states e_3 and e_2. Finally, it is worth noting that the knowledge of the oscillator strengths for the selected transitions allows determining the IR spectrum of water at any temperature according to Eq. (23).

IV. SUMMARY AND CONCLUSIONS

In this work, we introduced the possibility to calculate anharmonic absorption intensities of vibrational spectra by means of semiclassical dynamics. This is an important step in the direction of a complete description of infrared spectroscopy with respect to the power spectra simulations routinely provided by SC approaches. The goal has been achieved by using harmonic vibrational states as reference states to be evolved using the SC propagator (instead of the commonly employed coherent states). In fact, by Fourier transforming the SC recurring time-dependent overlap of harmonic states, the vibrational eigenfunctions can be obtained through a decomposition on the harmonic basis and the approach is readily extendable to high dimensional molecules. A successful application of the method, though, necessitates that the eigenfunctions obtained within the harmonic approximation give already a good qualitative representation. In fact, we showed that, in these cases, the most important anharmonic effects are already included with only very few terms in the harmonic basis set.

In the spirit of multiple coherent semiclassical dynamics, we propagated just one trajectory per anharmonic state so that the number of classical MD propagations is not directly related to the size of the molecule but to the number of vibrational target states. Once the trajectory associated with a target state has been propagated, the semiclassical propagator is determined for all harmonic basis functions needed to describe that specific state. The number of basis functions to employ depends on the dimensionality of the system, but it can be limited by employing an appropriate cutoff.

Test calculations performed on the 1D Morse oscillator have shown that the harmonic basis is very well suited to describe the true anharmonic vibrational states. In fact, all principal effects of anharmonicity generally present in bond stretching vibrations are captured by including only a few states in the harmonic expansion. Furthermore, excellent accuracy of the eigenfunctions (compared with their analytical representation used as a reference) is obtained after a simple post-processing refinement consisting in a Gram-Schmidt orthonormalization.

The formalism was applied to the H_2O molecule and we demonstrated that also in this case very high quality eigenfunctions (upon comparison to the DVR benchmarks) are obtained with a number of expansion coefficients of the order of one dozen. The presence of two main effects due to anharmonicity has been pointed out using our method: (i) the symmetric bond stretch actually provides an asymmetric contribution that shifts the wavefunctions in the direction of bond dissociation with respect to the harmonic counterparts, and (ii) a Fermi resonance arises between the fundamental of the symmetric stretch and the overtone of the bending. The relevance of both effects has been easily quantified on the basis of the harmonic expansion coefficients.

Another advantage of the functional form of the harmonic basis is that all the eigenfunctions are proportional to a multivariate Gaussian function. We took advantage from this to compute the vibrational intensities using a Monte Carlo strategy. First a number of the order of a few thousand molecular configurations is generated at negligible computational cost. Then, more expensive calculations are required to evaluate, for each structure generated, the total molecular dipole (e.g., via an *ab initio* self-consistent field calculation). This procedure, given the good level of scalability of the MC integration, can be directly extended to high dimensional systems with an affordable computational cost. For the cases in which the application of this protocol is anyway too demanding, we suggest (see Appendix B) a way to derive an approximate estimate of the anharmonic oscillator strengths using a linear expansion of the dipole operator. This approximation is commonly adopted to derive oscillator strengths in the harmonic approximation, and it just requires calculation of the first-order derivatives of the dipole expectation value (a common output in most quantum chemistry packages).

SUPPLEMENTARY MATERIAL

See supplementary material for additional data about the expansion coefficients and eigenenergies, and additional eigenfunction plots.

ACKNOWLEDGMENTS

Professor Tucker Carrington is warmly thanked for reading the manuscript and for interesting comments, and Dr. Gianluca Bertaina is thanked for insights about the Monte Carlo application. The authors acknowledge financial support from the European Research Council (ERC) under the European Union's Horizon 2020 research and innovation programme [Grant Agreement No. (647107)—SEMICOMPLEX—ERC-2014-CoG]. We thank Università degli Studi di Milano for computational time at CINECA (Italian Supercomputing Center) and CINECA under the Iscra-B (Grant QUASP) initiative for further computational time.

APPENDIX A: ANALYTICAL OVERLAP OF COHERENT AND HARMONIC STATES

We derive analytically the result reported in Eq. (22) for the one-dimensional scalar product $\langle \phi_k | \tilde{Q}, \tilde{p} \rangle$ between the coherent state $|\alpha\rangle$ centered in $(\tilde{Q}, \tilde{p})$ and the harmonic state of order k $|\phi_k\rangle$. This is easily derived considering that coherent states are eigenstates of the harmonic oscillator annihilation

operator $\hat{a} = \sqrt{\frac{\omega}{2\hbar}}\left(\hat{Q} + \frac{i}{\omega}\hat{p}\right)$,

$$\hat{a}|\alpha\rangle = \alpha|\alpha\rangle, \tag{A1}$$

where

$$|\tilde{Q}, \tilde{p}\rangle = N_\alpha e^{i\eta_\alpha}|\alpha\rangle \tag{A2}$$

with

$$\alpha = \sqrt{\frac{\omega}{2\hbar}}\,\tilde{Q} \;+\; i\sqrt{\frac{1}{2\omega\hbar}}\,\tilde{p}. \tag{A3}$$

In fact, by writing the coherent states in this convenient form, the scalar product with the harmonic state is also straightforwardly derived as

$$\langle\phi_k|\alpha\rangle = e^{i\eta_\alpha} e^{-\frac{|\alpha|^2}{2}} \frac{(\alpha)^k}{\sqrt{k!}}, \tag{A4}$$

and the only term that remains unknown is the phase factor η_α needed to get to the coherent state definition in Eq. (19). This is found comparing the scalar product between two coherent states,

$$\langle Q_1, p_1|Q_2, p_2\rangle = e^{i(\eta_{\alpha_2} - \eta_{\alpha_1})}\langle\alpha_1|\alpha_2\rangle, \tag{A5}$$

where $\alpha_1 = \sqrt{\frac{\omega}{2\hbar}}Q_1 + i\sqrt{\frac{1}{2\omega\hbar}}p_1$ and $\alpha_2 = \sqrt{\frac{\omega}{2\hbar}}Q_2 + i\sqrt{\frac{1}{2\omega\hbar}}p_2$. The integral on the left hand side of Eq. (A5) can be computed analytically giving

$$\langle Q_1, p_1|Q_2, p_2\rangle = e^{-\frac{\omega}{4\hbar}(Q_1 - Q_2)^2} e^{-\frac{1}{4\omega\hbar}(p_1 - p_2)^2} e^{\frac{i}{\hbar}(Q_1 - Q_2)(p_1 + p_2)}, \tag{A6}$$

while the scalar product on the right hand side of Eq. (A5) is

$$\langle\alpha_1|\alpha_2\rangle = \sum_k \langle\alpha_1|\phi_k\rangle\langle\phi_k|\alpha_2\rangle = e^{-|\alpha_1|^2} e^{-|\alpha_2|^2} e^{\alpha_1^* \alpha_2}. \tag{A7}$$

Inserting the results of Eq. (A6) and Eq. (A7) into Eq. (A5), it is straightforward to obtain

$$e^{i(\eta_{\alpha_2} - \eta_{\alpha_1})} = e^{\frac{i}{2\hbar}(Q_1 p_1 - Q_2 p_2)}, \tag{A8}$$

and hence, for the generic scalar product in Eq. (A4), it has to be

$$\eta_\alpha \;=\; -\frac{1}{2\hbar}\tilde{Q}\,\tilde{p}. \tag{A9}$$

APPENDIX B: APPROXIMATE APPROACH TO THE CALCULATION OF OSCILLATOR STRENGTHS IN HIGH DIMENSIONAL SYSTEMS

In view of the application of our methodology to the calculation of the oscillator strengths for high dimensional molecular systems, where the Monte Carlo sampling can become computationally demanding, it is worth noting that the integral in Eq. (29) can be evaluated in an approximate way without any further sampling of the molecular configurational space. This is achieved by considering the common linear expansion of the molecular dipole,

$$\mu_{0N}(\mathbf{q}) - \mu_{0N}(\mathbf{q}_{eq}) \simeq \sum_{\alpha=1}^{N_v} \left.\frac{\partial \mu_{0N}}{\partial q_\alpha}\right|_{\mathbf{q}_{eq}} (q_\alpha - q_{eq,\alpha}) = \mathbf{Z}_q \cdot \mathbf{Q}, \tag{B1}$$

where $\mathbf{Z}_q = \frac{\partial \mu_{0N}}{\partial q_\alpha}|_{\mathbf{q}_{eq}}$. Using this linearization, the transition dipoles can be obtained directly from the expansion of the eigenstates in the harmonic basis derived with the SC calculation

$$\langle e_n|\hat{Q}_\alpha|e_m\rangle = \sum_{\mathbf{K},\mathbf{K}'} C_{n,\mathbf{K}} C_{m,\mathbf{K}'} \langle\mathbf{K}|\hat{Q}_\alpha|\mathbf{K}'\rangle \tag{B2}$$

and by computing the transition dipoles on the harmonic states using the following relation:

$$\langle\mathbf{K}|\hat{Q}_\alpha|\mathbf{K}'\rangle = \left(\prod_{\beta\neq\alpha}^{N_v} \delta_{K_\beta, K'_\beta}\right)\sqrt{\frac{1}{2\omega_\alpha}} \times \left(\delta_{K_\alpha+1, K'_\alpha}\sqrt{K_\alpha + 1} + \delta_{K_\alpha - 1, K'_\alpha}\sqrt{K_\alpha}\right), \tag{B3}$$

which are immediately derived using the fact that $\hat{Q}_\alpha = \sqrt{\frac{1}{2\omega_\alpha}}\left(\hat{a}_\alpha^\dagger + \hat{a}_\alpha\right)$, with $\hat{a}_\alpha^\dagger$ and $\hat{a}_\alpha$, respectively, being the harmonic oscillator creation and annihilation operators for normal mode α.

[1] J. M. Bowman, T. Carrington, and H.-D. Meyer, Mol. Phys. **106**, 2145 (2008).
[2] V. Barone, M. Biczysko, J. Bloino, M. Borkowska-Panek, I. Carnimeo, and P. Panek, Int. J. Quantum Chem. **112**, 2185 (2011).
[3] A. P. Scott and L. Radom, J. Phys. Chem. **100**, 16502 (1996).
[4] K. K. Irikura, R. D. Johnson, and R. N. Kacker, J. Phys. Chem. A **109**, 8430 (2005).
[5] M.-P. Gaigeot, M. Martinez, and R. Vuilleumier, Mol. Phys. **105**, 2857 (2007).
[6] J. M. Bowman, S. Carter, and X. Huang, Int. Rev. Phys. Chem. **22**, 533 (2003).
[7] S. Carter, J. M. Bowman, and A. R. Sharma, AIP Conf. Proc. **1504**, 465 (2012).
[8] K. Yagi, M. Keceli, and S. Hirata, J. Chem. Phys. **137**, 204118 (2012).
[9] B. Thomsen, K. Yagi, and O. Christiansen, J. Chem. Phys. **140**, 154102 (2014).
[10] H.-D. Meyer, U. Manthe, and L. S. Cederbaum, Chem. Phys. Lett. **165**, 73 (1990).
[11] H.-D. Meyer and G. A. Worth, Theor. Chem. Acc. **109**, 251 (2003).
[12] G. Avila and T. Carrington, Jr., J. Chem. Phys. **147**, 144102 (2017).
[13] S. Manzhos and T. Carrington, J. Chem. Phys. **145**, 224110 (2016).
[14] R. Kosloff, Annu. Rev. Phys. Chem. **45**, 145 (1994).
[15] V. Barone, M. Biczysko, and J. Bloino, Phys. Chem. Chem. Phys. **16**, 1759 (2014).
[16] V. Barone, M. Biczysko, J. Bloino, and C. Puzzarini, Phys. Chem. Chem. Phys. **15**, 1358 (2013).
[17] A. Witt, S. D. Ivanov, M. Shiga, H. Forbert, and D. Marx, J. Chem. Phys. **130**, 194510 (2009).
[18] F. Mouhat, S. Sorella, R. Vuilleumier, A. M. Saitta, and M. Casula, J. Chem. Theory Comput. **13**, 2400 (2017).
[19] M. Schmidt and P.-N. Roy, J. Chem. Phys. **148**, 124116 (2018).
[20] G. Bertaina, D. E. Galli, and E. Vitali, Adv. Phys.: X **2**, 302 (2017).
[21] J. H. Van Vleck, Proc. Natl. Acad. Sci. U. S. A. **14**, 178 (1928).
[22] J. Cao and G. A. Voth, J. Chem. Phys. **104**, 273 (1996).
[23] W. H. Miller, J. Chem. Phys. **53**, 1949 (1970).
[24] W. H. Miller, J. Chem. Phys. **53**, 3578 (1970).
[25] W. H. Miller, in *Advances in Chemical Physics*, edited by I. Prigogine and S. A. Rice (John Wiley & Sons, Inc., 1974), Vol. 25.
[26] W. H. Miller, J. Phys. Chem. A **105**, 2942 (2001).
[27] E. J. Heller, J. Chem. Phys. **75**, 2923 (1981).
[28] M. F. Herman and E. Kluk, Chem. Phys. **91**, 27 (1984).
[29] K. G. Kay, J. Chem. Phys. **100**, 4377 (1994).
[30] N. Makri and W. H. Miller, J. Chem. Phys. **89**, 2170 (1988).
[31] H. Wang, D. E. Manolopoulos, and W. H. Miller, J. Chem. Phys. **115**, 6317 (2001).
[32] M. S. Church, S. V. Antipov, and N. Ananth, J. Chem. Phys. **146**, 234104 (2017).
[33] E. J. Heller, J. Chem. Phys. **94**, 2723 (1991).
[34] M. Šulc and J. Vaníček, Mol. Phys. **110**, 945 (2012).
[35] A. L. Kaledin and W. H. Miller, J. Chem. Phys. **118**, 7174 (2003).
[36] A. L. Kaledin and W. H. Miller, J. Chem. Phys. **119**, 3078 (2003).

[37]M. Buchholz, F. Grossmann, and M. Ceotto, J. Chem. Phys. **144**, 094102 (2016).
[38]M. Buchholz, F. Grossmann, and M. Ceotto, J. Chem. Phys. **147**, 164110 (2017).
[39]M. Buchholz, F. Grossmann, and M. Ceotto, J. Chem. Phys. **148**, 114107 (2018).
[40]M. Ceotto, S. Atahan, G. F. Tantardini, and A. Aspuru-Guzik, J. Chem. Phys. **130**, 234113 (2009).
[41]M. Ceotto, S. Atahan, S. Shim, G. F. Tantardini, and A. Aspuru-Guzik, Phys. Chem. Chem. Phys. **11**, 3861 (2009).
[42]M. Ceotto, D. Dell' Angelo, and G. F. Tantardini, J. Chem. Phys. **133**, 054701 (2010).
[43]M. Ceotto, G. F. Tantardini, and A. Aspuru-Guzik, J. Chem. Phys. **135**, 214108 (2011).
[44]M. Ceotto, S. Valleau, G. F. Tantardini, and A. Aspuru-Guzik, J. Chem. Phys. **134**, 234103 (2011).
[45]R. Conte, A. Aspuru-Guzik, and M. Ceotto, J. Phys. Chem. Lett. **4**, 3407 (2013).
[46]D. Tamascelli, F. S. Dambrosio, R. Conte, and M. Ceotto, J. Chem. Phys. **140**, 174109 (2014).
[47]M. Wehrle, M. Sulc, and J. Vanicek, J. Chem. Phys. **140**, 244114 (2014).
[48]F. Grossmann, J. Chem. Phys. **125**, 014111 (2006).
[49]M. Ceotto, G. Di Liberto, and R. Conte, Phys. Rev. Lett. **119**, 010401 (2017).
[50]G. Di Liberto, R. Conte, and M. Ceotto, J. Chem. Phys. **148**, 014307 (2018).
[51]F. Gabas, R. Conte, and M. Ceotto, J. Chem. Theory Comput. **13**, 2378 (2017).
[52]G. Di Liberto, R. Conte, and M. Ceotto, J. Chem. Phys. **148**, 104302 (2018).
[53]J. Tatchen and E. Pollak, J. Chem. Phys. **130**, 041103 (2009).
[54]V. S. Batista, M. T. Zanni, B. J. Greenblatt, D. M. Neumark, and W. H. Miller, J. Chem. Phys. **110**, 3736 (1999).
[55]G. Di Liberto and M. Ceotto, J. Chem. Phys. **145**, 144107 (2016).
[56]M. L. Brewer, J. S. Hulme, and D. E. Manolopoulos, J. Chem. Phys. **106**, 4832 (1997).
[57]Y. Zhuang, M. R. Siebert, W. L. Hase, K. G. Kay, and M. Ceotto, J. Chem. Theory Comput. **9**, 54 (2012).
[58]M. Ceotto, Y. Zhuang, and W. L. Hase, J. Chem. Phys. **138**, 054116 (2013).
[59]D. A. McQuarrie, *Statistical Mechanics* (Harper-Collins, 1976).
[60]W. H. Press, S. A. Teukolsky, W. T. Vetterling, and B. P. Flannery, *Numerical Recipes in FORTRAN; the Art of Scientific Computing*, 2nd ed. (Cambridge University Press, New York, NY, USA, 1993).
[61]B. Fornberg, *A Practical Guide to Pseudospectral Methods* (Cambridge University Press, 1998).
[62]S. Dressler and W. Thiel, Chem. Phys. Lett. **273**, 71 (1997).
[63]J. Suarez, S. Stamatiadis, S. C. Farantos, and L. Lathouwers, Comput. Phys. Commun. **180**, 2025 (2009).
[64]C. Lanczos, J. Res. Natl. Bur. Stand. **45**, 255 (1950).
[65]R. E. Wyatt, J. Chem. Phys. **103**, 8433 (1995).
[66]H. Guo, R. Chen, and D. Xie, J. Theor. Comput. Chem. **1**, 173 (2002).
[67]R. Guantes and S. C. Farantos, J. Chem. Phys. **111**, 10827 (1999).
[68]L. Lodi, J. Tennyson, and O. L. Polyansky, J. Chem. Phys. **135**, 034113 (2011).